

Example of exponentially enhanced magnetic reconnection driven by a spatially-bounded and laminar ideal flow

Allen H Boozer and Todd Elder
Columbia University, New York, NY 10027
ahb17@columbia.edu

(Dated: November 10, 2021)

In laboratory and natural plasmas of practical interest, the spatial scale Δ_d at which magnetic field lines lose distinguishability differs enormously from the scale a of magnetic reconnection across the field lines. In the solar corona, plasma resistivity gives $a/\Delta_d \sim 10^{12}$, which is the magnetic Reynolds number R_m . The traditional resolution of the paradox of disparate scales is for the current density j associated with the reconnecting field B_{rec} to be concentrated by a factor of R_m by the ideal evolution, so $j \sim B_{rec}/\mu_0\Delta_d$. A second resolution is for the ideal evolution to increase the ratio of the maximum to minimum separation between pairs of arbitrarily chosen magnetic field lines, $\Delta_{max}/\Delta_{min}$, when calculated at various points in time. Reconnection becomes inevitable where $\Delta_{max}/\Delta_{min} \sim R_m$. A simple model of the solar corona will be used for a numerical illustration that the natural rate of increase in time is linear for the current density but exponential for $\Delta_{max}/\Delta_{min}$. Reconnection occurs on a time scale and with a current density enhanced by only $\ln(a/\Delta_d)$ from the ideal evolution time and from the current density B_{rec}/μ_0a . In both resolutions, once a sufficiently wide region, Δ_r , has undergone reconnection, the magnetic field loses static force balance and evolves on an Alfvénic time scale. The Alfvénic evolution is intrinsically ideal but expands the region in which $\Delta_{max}/\Delta_{min}$ is large.

I. INTRODUCTION

Magnetic reconnection has an interesting early history [1] and was defined in 1956 by Parker and Krook [2] as the “*severing and reconnection of lines of force.*”

The ideal evolution of magnetic fields is the opposing concept to magnetic reconnection. Newcomb showed in 1958 that magnetic field lines move with a velocity \vec{u}_\perp and do not break, if and only if the field obeys the ideal evolution equation [3]

$$\frac{\partial \vec{B}}{\partial t} = \vec{\nabla} \times (\vec{u}_\perp \times \vec{B}). \quad (1)$$

The exact equation for the evolution of \vec{B} is Faraday’s Law, $\partial \vec{B}/\partial t = -\vec{\nabla} \times \vec{E}$. The ideal evolution of a magnetic field that is embedded in a plasma is broken [4] when the electric field parallel to the magnetic field, \vec{E}_\parallel , cannot be balanced by the parallel component of the gradient of a well-behaved potential, $\vec{\nabla} \cdot \Phi$. The components $\vec{E}_\perp + \vec{\nabla}_\perp \Phi$, which are perpendicular to \vec{B} , are associated with the velocity \vec{u}_\perp of the magnetic field lines, $\vec{u}_\perp = (\vec{E}_\perp + \vec{\nabla}_\perp \Phi) \times \vec{B}/B^2$.

Two effects that cause deviations from an ideal evolution are resistivity along the magnetic field η , which contributes to E_\parallel as $\eta \vec{j}_\parallel$, and electron inertia, which contributes [5] to E_\parallel as $(c/\omega_{pe})^2 \partial j_\parallel / \partial t$. The electron skin depth, c/ω_{pe} , is the speed of light divided by the electron plasma frequency.

The Oxford English Dictionary defines a paradox as “*a strongly counter-intuitive (statement), which*

investigation...may nevertheless prove to be well-founded or true.” Both the resistivity and the electron skin depth are so small in many plasmas of practical interest that it is paradoxical that magnetic reconnection could be of any relevance. Yet it is. Approximately 1500 papers have been written on magnetic reconnection, which demonstrate the importance of the topic to the understanding of both laboratory and naturally occurring plasmas. The speed and prevalence of magnetic reconnection are so great that they must be derivable from the properties of Equation (1) for the ideal evolution of a magnetic field [4].

To define the reconnection paradox, let a be a characteristic spatial scale over which u_\perp varies across the magnetic field lines; the time scale for an ideal evolution is

$$\tau_{ev} \equiv \frac{a}{u_\perp}, \quad (2)$$

Resistivity spatially interdiffuses magnetic field lines, which implies that lines that approach each other closer the distance $\Delta_d = \sqrt{(\eta/\mu_0)\tau_\eta}$ remain distinguishable only for a time t less than τ_η . The ratio of the resistive time scale of the overall system to the evolution time scale τ_{ev} is the magnetic Reynolds number

$$R_m \equiv \left(\frac{a^2}{\eta/\mu_0} \right) \left(\frac{u_\perp}{a} \right) = \frac{\mu_0 u_\perp}{\eta} a. \quad (3)$$

On the time scale τ_{ev} , magnetic field lines that come closer than $\Delta_d = a/R_m$ lose their distinguishability, where $R_m \sim 10^{12}$ in the solar corona.

The electron inertia causes evolving magnetic field lines that approach each other closer than $\Delta_d = c/\omega_{pe}$, the electron skin depth, to become indistinguishable, Appendix C of [6]. In the solar corona $a/(c/\omega_{pe}) \sim 10^9$.

What is paradoxical is that magnetic field lines are observed to reconnect and become indistinguishable over a region of width a across the magnetic field lines on a time scale only an order of magnitude or so longer than the characteristic ideal-evolution time of the magnetic field, τ_{ev} . Effects such as the resistivity would be expected to cause a loss of distinguishability of magnetic field lines in the solar corona only on a time scale of order 10^{12} times longer than τ_{ev} . This paradox was clearly described in 1988 by Schindler, Hesse, and Birn [7].

Schindler et al [7] sought to resolve the paradox of reconnection occurring over a region of far greater width than Δ_d . In their resolution, the current density would become and remain extremely large, $j \sim B_{rec}/(\mu_0\Delta_d)$, in a layer of width Δ_d , where B_{rec} is the part of the magnetic field that is reconnecting. This assumption has formed the basis of most of the reconnection literature from even before Schindler et al developed their reconnection theory. Nonetheless, it is difficult to understand how an ideal evolution would result in such a strong current. Most of the reconnection literature has not dealt with that issue but has focused instead on how such a large current density could be maintained if it were initially present. A foundational publication for recent work on the maintenance issue, with more than two hundred citations, is the 2010 paper by Uzdenksy, Louriero, and Schekochihin [8] on plasmoids.

The paradoxical speed of magnetic reconnection when non-ideal effects are extremely small has analogues with other phenomena such as thermal equilibration in air. The analogy between magnetic reconnection and thermal equilibration in a room was demonstrated [9] by Boozer in 2021. In both reconnection and thermal equilibration, the time scale of the relaxation of the ideal constraint is the ideal evolution time τ_{ev} times a term that is logarithmically dependent on the ratio of the non-ideal time scale divided by the τ_{ev} . This explains why a radiator can heat a room in tens of minutes rather than the several weeks that would be expected from thermal diffusion alone. Many may find the subtle mathematics used in [9] difficult to follow. Here a simple model of magnetic field evolution driven by footpoint motion, as in the solar corona, is used to illustrate the general principles that were explained in the companion paper [9].

The equation for temperature equilibration in air moving with a divergence-free velocity $\vec{v}(\vec{x}, t)$ is $\partial T/\partial t + \vec{v} \cdot \vec{\nabla} T = \vec{\nabla} \cdot (D\vec{\nabla} T)$, which is the stan-

dard form for the advection-diffusion equation. In many problems of practical importance, the Péclet number, va/D , is many orders of magnitude greater than unity. The diffusion coefficient for magnetic field lines is η/μ_0 , so the magnetic Reynolds number would be better called the magnetic Péclet number.

The classic paper on the advection-diffusion equation was written in 1984 by Hassan Aref [10] and has had over two thousand citations. This paper showed that a laminar flow can equilibrate T on the evolution time a/v times a logarithm of the Péclet number as $va/D \rightarrow \infty$. Before Aref's paper, it had been assumed a turbulent \vec{v} was required to obtain fast equilibration. Section I.B in an article [11] published in the Reviews of Modern Physics discusses the merits of the use of turbulent versus laminar flows to speed the mixing of fluids. What that article did not discuss is that for a given maximum flow speed v a laminar flow can give a faster mixing over a large region than a turbulent flow. A demonstration starts with the last sentence on p. 3 of [9]. Even when the overall flow is turbulent, it is the laminar part of the flow, which is defined by a spatial average over the turbulent eddies, that generally dominates the advective part of the advection-diffusion equation. Neither a turbulent nor a laminar flow directly produces diffusive mixing. Both exponentially enhance the speed with which diffusion can act over the spatial scale covered by the advection of the fluid.

The essential element in an enhanced relaxation by a laminar flow is that the flow be chaotic. Using standard terminology, a flow is deterministic but chaotic when neighboring streamlines have a separation that increases exponentially with time. Articles on the mathematics of deterministic chaos and topological mixing can easily be found on the web, but their importance to this paper is only that such effects are common. As noted in [9], although the condition that the flow be chaotic may sound restrictive, it is a non-chaotic natural flow that is essentially impossible to realize. No special effort is required to achieve enhanced mixing by stirring. Every cook knows that stirring enhances the mixing of fluids—no particular pattern of stirring or detailed computations are required.

The evolution equation for a magnetic field is also of the advection-diffusion type but more subtly so than the equation for thermal equilibration. The companion paper [9] derives two salient differences: (1) A flow-enhanced equilibration of the temperature requires a dependence of \vec{v} on at least two spatial coordinates to be energetically feasible, but flow-enhanced magnetic reconnection requires a dependence of \vec{u}_\perp on all three spatial coordinates for energetic feasibility. (2) In thermal relaxation, $|\vec{\nabla} T|$ increases exponentially with time but what one might

think would be the analogous quantity for the magnetic field, $\vec{j} = \vec{\nabla} \times \vec{B}/\mu_0$ does not. In the model developed in this paper, the increase in the current density is limited to being proportional to time. Related limits on the current density are known for resonant perturbations to toroidal plasmas [12] and for currents flowing near magnetic field lines that intercept a magnetic null [13].

When the ideal flow velocity of a magnetic field \vec{u}_\perp is chaotic, the ratio $\Delta_{max}/\Delta_{min}$, the maximum to the minimum separation between two field lines at any particular time, tends to increase exponentially during the evolution when the closest approach of the lines is small, $\Delta_{min}/a \rightarrow 0$. Large scale reconnection occurs for magnetic field lines that satisfy $\Delta_{min} \lesssim \Delta_d$ and $\Delta_{max} \approx a$. As will be seen, a simple laminar flow can be followed as $\Delta_{max}/\Delta_{min}$ increases by more than nine orders of magnitude.

The model that will be used to illustrate features of magnetic reconnection is developed in Section II. In this model, the magnetic field evolution is driven in a bounded plasma in the same way as footpoint motion drives the magnetic field in the solar corona.

Section III will show that when the footpoint velocity is sufficiently small compared to the Alfvén speed in the plasma that important features can be determined without solving the difficult problem of determining $\vec{B}(\vec{x}, t)$ throughout the plasma. These features include the exponentiation in time of the separation between neighboring magnetic field lines and the current density j_\parallel along each magnetic field line, or more precisely $K \equiv \mu_0 j_\parallel / B$. A bound on the magnitude of K is obtained, which increases linearly in time. For these features, only the determination of the streamlines of a time-dependent flow in two dimensions is required.

The simplicity of the treatment given in Section III depends on the evolution being slow compared to the Alfvén transit time. This would be violated if the plasma became kink unstable. Section IV shows that the flow example introduced in Section II ensures kink stability.

Section V shows that the rate of production of the magnetic flux associated with a particular magnetic field line by the footpoint motion is the magnetic Reynolds number R_m times larger than its rate of destruction by resistivity. The sign of the flux differs from field line to field line in kink-stable evolutions, and the rate of flux production and destruction can be brought into balance by reconnection.

Section VI shows that even if the plasma becomes kink unstable, the magnetic helicity contained in the bounded plasma will increase without limit when $R_m \gg 1$ unless the footpoint motion obeys a constraint. If the plasma were unbounded, an ever increasing helicity would presumptively result in a

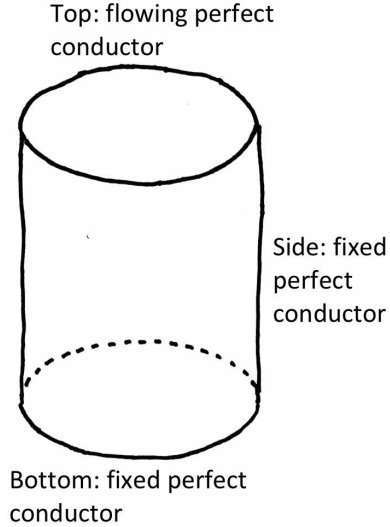


FIG. 1: A perfectly conducting cylinder of radius a and height L in z encloses an ideal pressureless plasma. All the sides of the cylinder are fixed except the top, which flows with a specified velocity \vec{v}_t . Initially, $\vec{B} = B_0 \hat{z}$.

plasma eruption.

Section VII derives the power that must be supplied to maintain the specified footpoint motion. For a steady-state flow, the required power increases linearly with K . Section VIII discusses the results and their implications.

II. MODEL OF THE SOLAR CORONA

Features of magnetic reconnection will be illustrated using a simplified model of magnetic loops in the solar corona. The evolution of coronal loops is driven by the motion of their footpoints by photospheric flows.

The description of the model has three parts: (1) Section II A defines a spatially bounded perfectly-conducting cylinder that encloses the loop as well as the flow \vec{v}_t in the top surface of the cylinder, which represents the photospheric motion. (2) Section II B explains the specific form chosen for \vec{v}_t . (3) Section II C explains how the chaotic properties of \vec{v}_t are quantified.

The numerical results for the streamlines of the flow \vec{v}_t are given in Section II D.

A. Definition of cylindrical region

The model that will be used to illustrate important features of magnetic reconnection consists an ideal pressureless plasma enclosed by a perfectly con-

ducting cylinder of radius a and height L , Figure 1. An ideal plasma means Equation (1) for an ideal magnetic evolution holds exactly. The conducting surfaces of the cylinder are rigid except for a flowing top-surface, which provides the footpoint motion that drives the evolution.

The flow of the top surface of the cylinder must be divergence free to avoid compressing the initial magnetic field $\vec{B}_0 = B_0 \hat{z}$ with B_0 a constant. The implication is the flow must have the form

$$\vec{v}_t = \hat{z} \times \vec{\nabla} h_t(x, y, t), \quad (4)$$

where the stream function h_t is chosen to represent a photospheric-like motion at one interception of a coronal magnetic loop. For simplicity, the flow at the other photospheric interception is taken to be zero. The effect of the flow is to produce a magnetic field orthogonal to \vec{B}_0 .

The model illustrated in Figure 1 is closely related to the well-known Parker Problem [14], which was recently reviewed by Pontin and Hornig [15]. It is also a simplified version of reconnection models of the corona published by Boozer [16] and independently by Reid et al [17] in 2018. Although these two models are similar, the mathematical cause for reconnection emphasized in these papers is different. Reid et al [17] used an anomalous resistivity to ensure “*that resistivity, as opposed to a numerical diffusion, is responsible for any magnetic reconnection.*” Boozer’s paper and his more recent work [4, 6, 9, 18] emphasized that an imposed chaotic flow \vec{v}_t would make magnetic reconnection exponentially sensitive to any departures from an ideal evolution—even effects due to numerics rather than physics.

B. Choice of \vec{v}_t

The divergence-free velocity \vec{v}_t is specified by the stream function $h_t(x, y, t)$, Equation (4). Using Cartesian coordinates, the stream function is the Hamiltonian for the streamlines of the flow on the top of the cylinder $dx/dt = -\partial h_t/\partial y$ and $dy/dt = \partial h_t/\partial x$.

The flow should satisfy certain conditions, and these are easier to impose in cylindrical coordinates r, θ, z where $x = r \cos \theta$ and $y = r \sin \theta$. The vertical part of the cylindrical shell is at $r = a$. The stream function h_t should be chosen so h_t , dr/dt , $d\theta/dt$, and the radial gradient of $d\theta/dt$ are all zero at $r = a$. This ensures that the streamlines can never strike the $r = a$ boundary of the cylinder, $\vec{v}_t = 0$ at $r = a$, and extremely large currents do not form in the plasma near $r = a$.

A form for h_t that satisfies these conditions is

$$h_t(r, \theta, t) = \tilde{h}(x, y, t) \left(1 - \frac{r^2}{a^2}\right)^3 e^{-\lambda^2 r^2/a^2}, \quad (5)$$

where λ^2 is a constant. A large λ^2 restricts the evolution-driven region to be far from the confining cylindrical walls. In the studies reported here, $\lambda^2 = 0$. The stream function h_t is fully specified when $\tilde{h}(x, y, t)$ is given.

Flows that carry footpoints over a scale comparable to a are the most effective at producing a rapid reconnection [9]. These are slowly varying terms in x and y , which in simple forms are

$$\tilde{h} = \frac{a^2}{\tau} \left[c_0 \cos\left(\omega_0 \frac{t}{\tau}\right) + c_1 \frac{x}{a} \cos\left(\omega_1 \frac{t}{\tau}\right) + c_2 \frac{y}{a} \sin\left(\omega_2 \frac{t}{\tau}\right) \right] + c_3 \frac{xy}{a^2} \cos\left(\omega_3 \frac{t}{\tau}\right), \quad (6)$$

where ω_0 , ω_2 , and ω_3 are three frequencies, which are generally incommensurate, and c_0 , c_1 , c_2 , and c_3 are dimensionless amplitudes. The amplitudes and frequencies used in the calculations are $c_0 = 0$, $c_1 = c_2 = c_3 = 1/4$, $\omega_1 = 6\pi$, $\omega_2 = 4\pi$, and $\omega_3 = 0$.

The c_0 term by itself would produce streamlines that lie on circles, which produce a large parallel current density with a long correlation distance. Such current densities tend to be ideal-kink unstable, Section IV, which would violate the assumption of a slow evolution compared to Alfvénic. As will be shown in Section III the analysis is greatly simplified when the evolution is slow compared to Alfvénic. Consequently, the coefficient c_0 was chosen to be zero. As shown by Reid et al [19], the kinks produced by pure circular motions lead to a large scale exponential separation of neighboring magnetic field lines. The only reason for choosing $c_0 = 0$ is to be able to study a rigorously correct but simple example.

For determining the chaotic region associated with a particular initial condition x_0, y_0 , it is advantageous for the frequencies to be commensurate because then a Poincaré plot can be constructed using the time-periodic points. When the frequencies are commensurate, τ is the periodicity or transit time of \tilde{h} . The exponentiation, which as explained in Section IIC is measured by the Frobenius norm, can be calculated whether the frequencies are commensurate or not.

The actual value of τ is arbitrary. It is effectively the unit of time. Similarly the distance L can be chosen arbitrarily. Only dimensionless ratios are important. The Alfvén speed V_A only enters through the constraint, $L/\tau \ll V_A$.

A circular conducting-cylinder is easier to discuss and does not complicate the computations of this

paper, but a cylinder with a square cross section simplifies more complete simulations. In a square cylinder, the factors of $1 - r^2/a^2$ in Equation (5) are replaced by $(1 - x^2/a^2)(1 - y^2/a^2)$.

C. Quantification of chaos

The stream function h_t is the Hamiltonian for the stream lines of the flow \vec{v}_t with (x, y) the canonical variables. The most important question about a specific flow is whether its streamlines are chaotic.

Neighboring chaotic streamlines have a separation $\vec{\delta}$ that depends exponentially on time. Neighboring means separated by an infinitesimal distance. The exponentiation of neighboring streamlines can be defined streamline by streamline. The $t = 0$ location of a streamline (x_0, y_0) defines that streamline, which at time t has the position $\vec{x} = x(x_0, y_0, t)\hat{x} + y(x_0, y_0, t)\hat{y}$, where $(\partial\vec{x}/\partial t)_{x_0y_0} \equiv d\vec{x}/dt = \vec{v}_t$.

To determine not only the streamline that is at (x_0, y_0) at $t = 0$ but also all the streamlines in its neighborhood two vector equations should be integrated simultaneously:

$$\frac{d\vec{x}}{dt} = \vec{v}_t, \text{ where} \quad (7)$$

$$\vec{v}_t = -\frac{\partial h_t}{\partial y}\hat{x} + \frac{\partial h_t}{\partial x}\hat{y}, \text{ and} \quad (8)$$

$$\frac{d\vec{\delta}}{dt} = \vec{\delta} \cdot \vec{\nabla} \vec{v}_t. \quad (9)$$

Equation (7) is to be solved with the initial condition $\vec{x}(0) = x_0\hat{x} + y_0\hat{y}$, so solving that equation means solving two coupled equations, one for dx/dt and one for dy/dt .

Equation (9) for $\vec{\delta}$ is obtained from the equation for neighboring magnetic field lines, which solve the exact equation $d(\vec{x} + \vec{\delta})/dt = \vec{v}_t(\vec{x} + \vec{\delta}, t)$, by taking the limit as $|\vec{\delta}| \rightarrow 0$. Equation (9) should be solved for two different initial conditions. The first solve is for $\vec{\delta}_x = \delta_{xx}\hat{x} + \delta_{xy}\hat{y}$ with the initial condition $\delta_{xx} = 1$ and $\delta_{xy} = 0$. The second solve is for $\vec{\delta}_y = \delta_{yx}\hat{x} + \delta_{yy}\hat{y}$ with the initial condition $\delta_{yx} = 0$ and $\delta_{yy} = 1$. Since Equation (9) for the evolution of the separation $\vec{\delta}$ is linear, the initial separation can be taken to be unity without loss of generality.

The Jacobian matrix for the starting point (x_0, y_0) , which is defined by

$$\frac{\partial\vec{x}}{\partial\vec{x}_0} \equiv \begin{pmatrix} \frac{\partial x}{\partial x_0} & \frac{\partial x}{\partial y_0} \\ \frac{\partial y}{\partial x_0} & \frac{\partial y}{\partial y_0} \end{pmatrix} \text{ is then} \quad (10)$$

$$= \begin{pmatrix} \delta_{xx} & \delta_{xy} \\ \delta_{yx} & \delta_{yy} \end{pmatrix}. \quad (11)$$

The determinant of the Jacobian matrix, $\delta_{xx}\delta_{yy} - \delta_{yx}\delta_{xy}$, called the Jacobian, would be unity if there were no numerical errors. This follows from Liouville's theorem of Hamiltonian mechanics.

The Frobenius norm of a matrix is the square root of the sum of the squares of the matrix elements and is also equal to the sum of the squares of the singular values of a Singular Value Decomposition (SVD) of the matrix. The Jacobian of a matrix is the product of its singular values, and a 2×2 matrix has two singular values Λ_u and Λ_s ; by definition $\Lambda_u \geq \Lambda_s$.

Consequently, the Frobenius norm of the Jacobian matrix, $\|\partial\vec{x}/\partial\vec{x}_0\|$, gives the large singular value, Λ_u , of a Singular Value Decomposition (SVD) of the matrix $\partial\vec{x}/\partial\vec{x}_0$:

$$\begin{aligned} \left\| \frac{\partial\vec{x}}{\partial\vec{x}_0} \right\| &\equiv \sqrt{\delta_{xx}^2 + \delta_{xy}^2 + \delta_{yx}^2 + \delta_{yy}^2}; \\ &= \sqrt{\Lambda_u^2 + 1/\Lambda_u^2} \end{aligned} \quad (12)$$

since $\Lambda_s = 1/\Lambda_u$.

When the flow is chaotic, neighboring streamlines separate exponentially, and Λ_u becomes exponentially large, which means Λ_u is essentially equal to the Frobenius norm of the Jacobian matrix, $\|\partial\vec{x}/\partial\vec{x}_0\|$. A full SVD analysis gives additional information, the directions in both x_0, y_0 space and in x, y space in which trajectories exponentiate apart and exponentiate together.

The numerical accuracy of the calculations, which are based on Runge-Kutta integrations, can be checked not only by the deviation of the Jacobian from unity, but also by simultaneously integrating one additional equation, $dh_t/dt = \partial h_t/\partial t$, and finding the deviation of h_t resulting from the integration from the actual h_t .

The Frobenius norm of the Jacobian matrix is used here to define the magnitude of the exponentiation. This norm involves a sum of positive numbers and is less numerically demanding than calculating the SVD or the Jacobian, which is the difference between two numbers, each of order the Frobenius norm squared. The largest Frobenius norm in this paper is approximately 10^8 . The Jacobian can be the difference between two terms each of order 10^{16} . The maximum error in the Jacobian is 15%. A more representative number is the standard deviation of the Jacobian from unity, which is 1.1%.

D. Numerical results for the streamlines of \vec{v}_t

Figure 2a illustrates the effect of a simple \vec{v}_t that is chaotic, as almost all choices of h_t that have non-trivial x, y , and t dependencies are. One hundred streamlines are started on the perimeter of the small

a. A Hundred Initial(black)/Final(red) Streamline Locations b. A Hundred Frobenius Norms c. A Hundred Currents

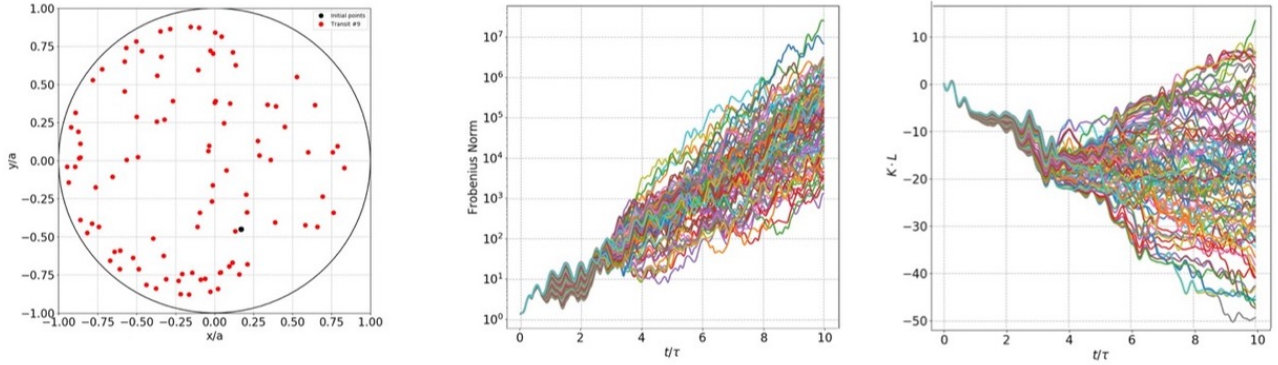


FIG. 2: Streamline properties are illustrated for the stream function of Equation (6) with $c_0 = 0$, $c_1 = c_2 = c_3 = 1/4$, $\omega_1 = 6\pi$, $\omega_2 = 4\pi$, $\omega_3 = 0$, and $\lambda^2 = 0$. Figure 2a is plot of a hundred streamlines started on the perimeter of the small black circle, which has a radius of $a/100$ and is centered at an arbitrary point, $x/a = 0.17$ and $y/a = -0.45$. The red dots are the locations of the hundred streamlines after nine transits. The locations are widely scattered within the region $r < a$ in which the derivatives of the stream function are non-zero. Figure 2b shows the evolution of the Frobenius norm, Equation (12) for these hundred streamlines. The Frobenius norm is a precise measure of the separation of neighboring trajectories. As expected in a chaotic flow, the Frobenius norm tends to increase exponentially with time. Figure 2c shows the evolution of the force-free current $K \equiv \mu_0 j_{||} / B$ times the length of the cylinder L given by Equation (35) for each of the hundred field lines that initially intercepted the top surface on the perimeter of the black circle.

A Thousand Points on Small Circles

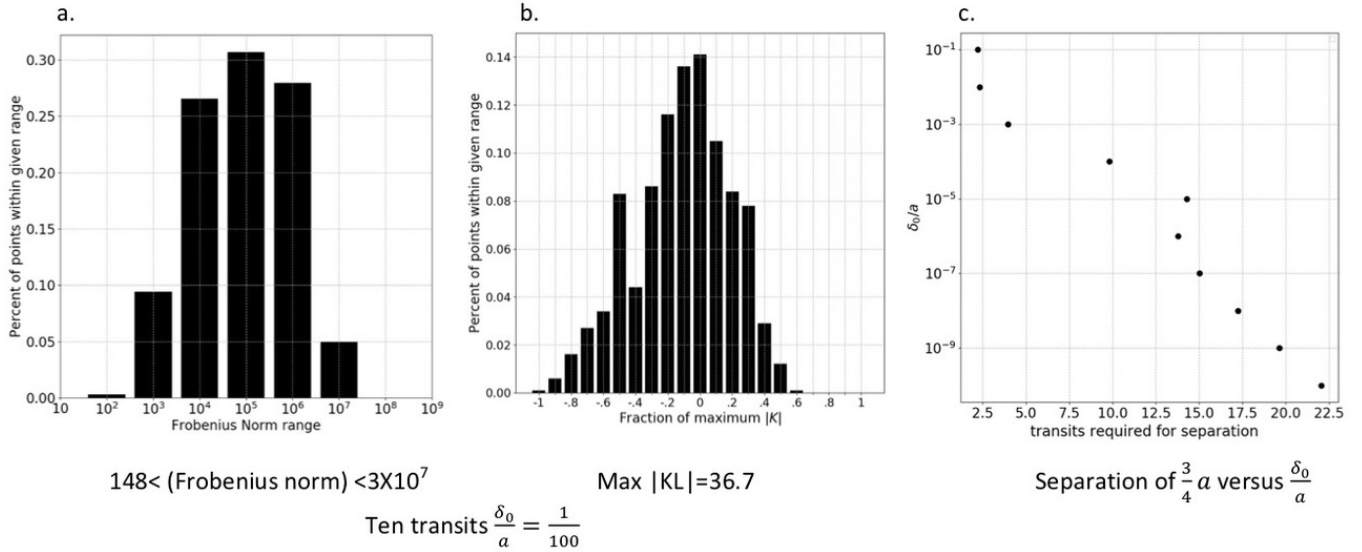


FIG. 3: Data was gathered from a thousand starting points on the perimeter of a circle of radius δ_0 . Figure 3a shows the frequency of occurrence of different values of Frobenius norm when $\delta_0 = a/100$. The same value as in Figure 2. Figure 3b shows the frequency of occurrence of different values of the current K , positive and negative, when $\delta_0 = a/100$. Figure 3c shows the logarithmic scaling of the number of transits required for points started on the perimeter of a circle of radius δ_0 to reach the scale $3a/4$. Figures 3a and 3b used data from ten transits.

Ten Thousand Uniformly Spread Points over $r < a$ Followed Ten Transits

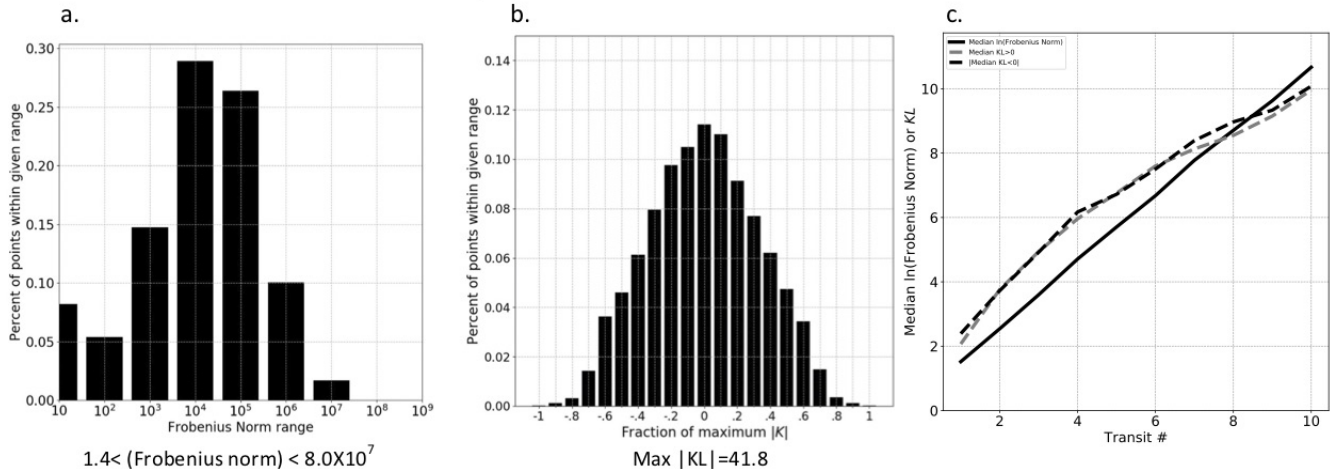


FIG. 4: Ten thousand starting points were uniformly spread over $r < a$. Figure 4a is the frequency with which streamlines have various values of the Frobenius norm. Figure 4b is the distribution of the current, both positive and negative, relative to the maximum $|KL| = 41.8$. Figure 4c relates the median value of the natural logarithm of the Frobenius norm (solid line), the median value the positive KL magnitudes, and the median value of the negative KL magnitudes.

black circle, but as the red dots illustrate, these hundred streamlines spread over most of the region $r < a$ after only five periods τ of the flow. The perimeter of the small circle defines a tube in time with fixed area. The cross section of this tube becomes convoluted in the extreme; all the red dots must lie on the perimeter of the tube. Figure 2b illustrates the evolution of the Frobenius norms of these hundred streamlines. Figure 3a gives the frequency distribution of the Frobenius norms for a thousand streamlines started on the small black circle. The smallest Frobenius norm for these thousand streamlines is 148 and the largest is 3×10^7 . The frequency distribution is peaked near their geometric mean $\sqrt{(148) \times (3 \times 10^7)} \approx 6.7 \times 10^4$.

A thousand streamlines were launched from a circle of radius δ_0 and the number of transits, t/τ , was recorded for the streamlines to become separated by a distance $3a/4$. Figure 3c shows that the required number of transits is proportional to the logarithm of the chosen δ_0 .

The fraction of the total $r < a$ region that has chaotic streamlines is assessed by starting a thousand streamlines at uniformly spread points over the $r < a$ region and following them for ten transits. The frequency with which various Frobenius norms arose is shown in Figure 4a. The smallest Frobenius norm is $\sqrt{2}$, which is the smallest value that is mathematically allowed. The peak at small Frobenius norms implies that non-chaotic regions exist, which are separated by Lagrangian coherent structures from the chaotic regions [20]. In non-chaotic

regions, the separation between neighboring streamlines typically increases in proportion to time. The frequency distribution of Frobenius norms is peaked near the geometric mean, 1.1×10^4 , of the largest, 8×10^7 , and the smallest Frobenius norm.

The fractional distribution of exponentiations in the separation of magnetic field lines was calculated in 2014 for a related problem by Huang et al [21] with far fewer e-folds; their distribution was also peaked.

III. EVOLUTION EQUATIONS

The magnetic field evolution in the model described in Section II becomes remarkably simple when the height of the cylinder is far greater than its radius, $L/a \rightarrow \infty$ and the time scale of ideal evolution is very long compared the the Alfvén transit time. For simplicity the plasma pressure is assumed to be zero. The derivation is essentially a simplified version of the derivation of Reduced MHD [22, 23].

This section consists of four subsections. The first two subsections, Section III A and III B, derive two differential equations that relate the Lagrangian derivatives of time and distance along the magnetic field lines ℓ of the distribution of parallel current $K \equiv \mu_0 j_{||} / B$ and the vorticity $\Omega \equiv \hat{z} \cdot \nabla \times \vec{u}_{\perp}$ of the magnetic field line flow. The third subsection, Section III C, discusses the implications of these two equations and is the most important part of the paper. The fourth subsection, Section III D, gives a heuristic argument that the magnitude of the cur-

rent distribution K should typically scale as the strength of the exponential separation of the magnetic field lines, their Frobenius norm. This relation is shown to hold accurately for the ensemble of many field lines but not for each line. Indeed, the correlation between large values of K and large values of the Frobenius norm is found to be remarkably weak.

A. Simplification of the magnetic evolution

When $L/a \rightarrow \infty$, the magnetic field consists of a constant field B_0 in the \hat{z} direction plus an orthogonal field produced by the velocity in the top surface. $\vec{\nabla} \cdot \vec{B} = 0$ implies the magnetic field and the vector potential have the forms

$$\vec{B} = B_0 \left(\hat{z} + \hat{z} \times \vec{\nabla} H \right); \quad (13)$$

$$\vec{A} = B_0 \left(\frac{\hat{z} \times \vec{x}}{2} - H \hat{z} \right), \quad (14)$$

where $\vec{B} = \vec{\nabla} \times \vec{A}$.

Equation (1) for the ideal evolution of the magnetic field implies the vector potential evolves as

$$\frac{\partial \vec{A}}{\partial t} = \vec{u}_\perp \times \vec{B} - B_0 \vec{\nabla} h, \quad (15)$$

where $B_0 = \hat{z} \cdot \vec{B}$ is a constant and h represents the freedom of gauge. The constraint that the \hat{z} -directed field does not change is

$$\hat{z} \cdot \frac{\partial \vec{B}}{\partial t} = -\vec{\nabla} \cdot \left(\hat{z} \times \frac{\partial \vec{A}}{\partial t} \right) = 0. \quad (16)$$

A vector identity implies $\hat{z} \times (\vec{u}_\perp \times \vec{B}) = (\hat{z} \cdot \vec{B}) \vec{u}_\perp - (\hat{z} \cdot \vec{u}_\perp) \vec{B}$. Consequently, the constraint on the constancy of $B_0 = \hat{z} \cdot \vec{B}$ is that the velocity of the magnetic field lines have the form

$$\vec{u}_\perp = \hat{z} \times \vec{\nabla} h. \quad (17)$$

The curl of the magnetic field of Equation (13) and the curl of the magnetic field line velocity \vec{u}_\perp of Equation (17) give the current and the vorticity along \vec{B} :

$$\nabla_\perp^2 H = K, \text{ where } K \equiv \frac{\mu_0 j_{\parallel}}{B}, \text{ and} \quad (18)$$

$$\nabla_\perp^2 h = \Omega, \text{ where } \Omega \equiv \hat{z} \cdot \vec{\nabla} \times \vec{u}_\perp. \quad (19)$$

Equations (14) and (15) give two expressions for $\vec{B} \cdot (\partial \vec{A} / \partial t)_{\vec{x}}$, which can be equated to obtain

$$\frac{\partial H}{\partial t} = \frac{\vec{B} \cdot \vec{\nabla} h}{B_0} \quad (20)$$

$$= \frac{\partial h}{\partial z} + (\hat{z} \times \vec{\nabla}_\perp H) \cdot \vec{\nabla}_\perp h \quad (21)$$

$$= \frac{\partial h}{\partial z} + \hat{z} \cdot (\vec{\nabla}_\perp h \times \vec{\nabla}_\perp H). \quad (22)$$

Applying ∇_\perp^2 to both sides of this equation,

$$\begin{aligned} \frac{\partial \nabla_\perp^2 H}{\partial t} &= \frac{\partial \nabla_\perp^2 h}{\partial z} + \hat{z} \cdot (\vec{\nabla}_\perp \nabla_\perp^2 h \times \vec{\nabla}_\perp H) \\ &\quad + \hat{z} \cdot (\vec{\nabla}_\perp h \times \vec{\nabla}_\perp \nabla_\perp^2 H) \end{aligned} \quad (23)$$

$$= \frac{\vec{B}}{B_0} \cdot \vec{\nabla} (\nabla_\perp^2 h) - \vec{u}_\perp \cdot \vec{\nabla}_\perp (\nabla_\perp^2 H). \quad (24)$$

These equations and the definition of K , Equation (18), and of Ω , Equation (19), imply

$$\left(\frac{\partial K}{\partial t} \right)_L = \left(\frac{\partial \Omega}{\partial \ell} \right)_L, \quad (25)$$

where the subscript L on the partial derivatives implies the use of Lagrangian coordinates, which means x_0 and y_0 are held constant;

$$\left(\frac{\partial K}{\partial t} \right)_L \equiv \frac{\partial K}{\partial t} + \vec{u}_\perp \cdot \vec{\nabla} K, \text{ and} \quad (26)$$

$$\left(\frac{\partial \Omega}{\partial \ell} \right)_L \equiv \vec{B} \cdot \vec{\nabla} \Omega. \quad (27)$$

The differential distance along a magnetic field line, $d\ell$, is equivalent to dz with x_0 and y_0 held constant.

The implications of Equation (25) will be found to be extremely profound.

B. Constraint of force balance

The Lagrangian time and ℓ derivatives of the parallel current distribution $K \equiv \mu_0 j_{\parallel} / B$ and the vorticity Ω obey not only Equation (25) but also Equation (31), which is implied by force balance.

For simplicity, the plasma is assumed to have a negligible pressure and a constant density ρ , so force balance is $\rho(\partial \vec{u}_\perp / \partial t + \vec{u}_\perp \cdot \vec{\nabla} \vec{u}_\perp) = \vec{f}_L$, where $\vec{f}_L \equiv \vec{j} \times \vec{B}$ is the Lorentz force. The condition $\vec{\nabla} \cdot \vec{j} = 0$ can be written as

$$\vec{B} \cdot \vec{\nabla} K = \vec{B} \cdot \vec{\nabla} \times \frac{\mu_0 \vec{j}_L}{B^2}, \text{ and} \quad (28)$$

$$\vec{\nabla} \times (\vec{u}_\perp \cdot \vec{\nabla} \vec{u}_\perp) = \vec{\nabla} \times (\vec{\Omega} \times \vec{u}_\perp) \quad (29)$$

$$= \vec{u}_\perp \cdot \vec{\nabla} \vec{\Omega} - \vec{\Omega} \cdot \vec{\nabla} \vec{u}_\perp, \quad (30)$$

where $\vec{\Omega} = \Omega \hat{z}$. The \hat{z} component of the curl of the force balance equation gives

$$\left(\frac{\partial \Omega}{\partial t} \right)_L = V_A^2 \left(\frac{\partial K}{\partial \ell} \right)_L, \text{ where } V_A^2 \equiv \frac{B_0^2}{\mu_0 \rho} \quad (31)$$

is the Alfvén speed.

C. Implications of the K and Ω equations

Equations (25) and (31) together with the mixed partials theorem applied to either Ω or K imply both Ω and K obey the equation for shear Alfvén waves, $(\partial^2 K / \partial t^2)_L = V_A^2 (\partial^2 K / \partial \ell^2)_L$. Any variation in K along the magnetic field lines relaxes by Alfvén waves. Reconnection or ideal kink-instabilities will generally drive Alfvén waves. The inclusion of resistivity or viscosity causes these waves to diffuse across the magnetic field lines and produces wave decay [25]. In a completely ideal theory, the energy that goes into Alfvén waves will bounce back and forth forever, but they can be damped without directly affecting reconnection by adding viscosity or a drag-force to the force equation.

Equations (25) and (31) imply that during any period in which the evolution is slow compared to the Alfvén transit time L/V_A that

$$\left(\frac{\partial K}{\partial \ell}\right)_L = 0, \text{ and} \quad (32)$$

$$\left(\frac{\partial^2 \Omega}{\partial \ell^2}\right)_L = 0, \text{ so} \quad (33)$$

$$\Omega = \Omega_t(x_0, y_0, t) \frac{\ell}{L}, \text{ and} \quad (34)$$

$$\left(\frac{\partial K}{\partial t}\right)_L = \frac{\Omega_t(x_0, y_0, t)}{L}, \text{ where} \quad (35)$$

$$\Omega_t \equiv \hat{z} \cdot \vec{\nabla} \times \vec{v}_t. \quad (36)$$

The flow of the top perfectly-conducting surface is specified, and $\Omega_t(x_0, y_0, t)$ is obtained from that specified flow alone. For an example of a calculation of the evolution of KL , see Figure 2c.

Equations (18) and (35) provide a Poisson equation, $\nabla_{\perp}^2 H = K$, for H and an expression for K , which can be solved for each value of z and t . The boundary condition is that the component of $\vec{\nabla}_{\perp} H$ that is tangential to the wall must vanish, otherwise the magnetic field would penetrate the perfectly conducting wall.

For any physically reasonable flow, $\Omega_t(x_0, y_0, t)$ is bounded, $|\Omega_t| \leq \Omega_{max}$, which can be easily calculated analytically for any analytic $h_t(x, y, t)$. An extremely important result is that the maximum current density along the magnetic field j_{\parallel} satisfies

$$K_{max} \leq \frac{\Omega_{max}}{L} t. \quad (37)$$

The fraction of the values of K that have a particular value is illustrated for magnetic field lines started on a small circle of radius $a/100$ in Figure 3b and for lines started uniformly over the full region, $r < a$ in Figure 4b. For the small circle, the

current K is more likely to be negative than positive, which is also clearly illustrated in Figure 2c, but nonetheless K 's of both signs are present. Over the full region, frequency distribution of currents, Figure 4b, is essentially symmetric between the negative and the positive values, and the most probable K is essentially zero. The absence of smoothness in the current distribution K , even in a small region, Figure 2c, due to a smooth flow may be surprising to some. An implication is that currents in the corona must be extremely complicated with a short correlation distance across the magnetic field lines.

When the specified flow in the top surface is chaotic, the spatial derivatives of K will tend to become exponentially large in some directions and exponentially small in others, but the current density itself is strictly bounded by a linear increase in time. In other words, the current density within the plasma lies in ribbons with a decreasing thickness in one direction across \vec{B} , an increasing width in the other direction across \vec{B} , and a constant amplitude along \vec{B} . This thinning with increasing width is illustrated by the top row of Figure 5.

The anisotropy of the spatial derivatives of K follows from the exponentially large anisotropy of the spatial derivatives of $\Omega_t(x_0, y_0, t)$ in x_0, y_0 space. For simple stream functions $h_t(x, y, t)$, such as those defined by Equation (6), $\Omega_t(x, y, t) = \nabla^2 h_t$ has a simple and smooth variation in x, y coordinates. But, the streamlines, $x(x_0, y_0, t)$ and $y(x_0, y_0, t)$, of a two-dimensional, divergence-free chaotic flow separate exponentially in time in one direction, which implies they must exponentially converge in the other. For a divergence-free flow, the two singular values of the Jacobian matrix $\partial \vec{x} / \partial \vec{x}_0$ must be inverses of each other. The spatial derivatives of $\Omega_t(x_0, y_0, t)$ in the converging direction become exponentially large and those in the diverging direction become exponentially small.

Employing Equation (35), $\Omega_t(x_0, y_0, t)$ determines the distribution of the parallel current density $K(x_0, y_0, z, t)$. Consequently, the streamlines of \vec{v}_t determine the properties of $K(x_0, y_0, z, t)$ throughout the plasma. In the limit $V_A \gg L/\tau$, the Lorentz force and, therefore, j_{\perp} are negligible. Figure 2c illustrates how a hundred magnetic field lines that initially had nearby x_0, y_0 locations develop a large variation in KL . As can be seen in Figure 5, there is only a weak correlation between regions where $|K|$ is large and where the Frobenius norm is large. This is consistent with the results of Reid et al [19] that the quasi-squashing factor, which is determined by the Frobenius norm, Equation (12), has a little correlation with a large $\int \eta j_{\parallel} d\ell = B_0(\eta/\mu_0)KL$.

Magnetic field lines that have distant intersection points with the bottom surface of the cylinder, x_0, y_0

and x'_0, y'_0 can interchange their intersections on the top surface if anywhere along their trajectories they are sufficiently close, $< \Delta_d$, to be indistinguishable. This means they come closer than c/ω_{pe} or the distance through which they resistively diffuse, $\sqrt{(\eta/\mu_0)t}$.

D. Required current density

The current density required for a large exponentiation is relatively small [26]. The minimum number of exponentiations is given by the properties of h_t , but more are possible. The separation $\vec{\Delta} = \Delta_x \hat{x} + \Delta_y \hat{y}$ between two neighboring magnetic field lines obeys $d\vec{\Delta}/dz = \vec{\Delta} \cdot \vec{\nabla} \hat{b}$, where $\hat{b} = \hat{z} + \hat{z} \times \vec{\nabla} H$. That is,

$$\frac{d\Delta_x}{dz} = -\frac{\partial^2 H}{\partial x \partial y} \Delta_x - \frac{\partial^2 H}{\partial y^2} \Delta_y \quad (38)$$

$$\frac{d\Delta_y}{dz} = \frac{\partial^2 H}{\partial x^2} \Delta_x + \frac{\partial^2 H}{\partial x \partial y} \Delta_y. \quad (39)$$

An exact answer for the separation requires a solution of the equation $\nabla_{\perp}^2 H = K$. But, the typical magnitude of the second derivatives of H , which appear in Equations (38) and (39) is K , which suggests that the number of e-folds is typically of order KL . Figure 2 illustrates this scaling, and Figure 4c shows the accuracy with which the scaling holds. Although the scaling holds for the ensemble averages, it does not hold magnetic field line by field line, which is another way of saying that the correlation between the magnitude of the Frobenius norm and the current density is weak, Figure 5. A current along a magnetic field line affects not only the Hamiltonian and its derivatives on that line but elsewhere as well.

IV. KINK STABILITY

The current flowing along the magnetic field lines causes the lines to twist through an angle $\Theta = KL/2$ from one end of the cylinder to the other. When the twist has a smooth variation with radius, Hood and Priest [27] found the magnetic field becomes unstable to an ideal kink when Θ is greater than a critical value, which in their calculations lay in the range 2π to 6π . Studies of the onset of reconnection in the model of Figure 1 are much simpler when ideal kink instabilities are not an issue.

The largest KL values in Figure 2c correspond to $\Theta \approx 8\pi$, but the current K has an extremely complicated spatial distribution, not only in magnitude but also in sign; spatial averages are far smaller than the maximum value. As will be discussed, the

anisotropy of the derivatives of K across the magnetic field lines and the smallness of the spatial averages of K makes the system highly stable to kinks.

It is not required that K , or equivalently the twist Θ , have small spatial averages when the flow is chaotic. The spatially averaged twist Θ can be made arbitrarily large by choosing c_0 to be large and ω_0 to be either zero or small in Equation (6) for \tilde{h} . The choice $c_0 = 0$ was made to show that a large average field line twist is not needed to obtain chaos.

Even when $c_0 = 0$, the spatial average of K over small regions can be non-zero. This is illustrated by Figure 2c and by the first row of Figure 5.

When the stream function is chosen so the flow is chaotic but with a large spatially-averaged K , the resulting magnetic field will generally evolve not only into a kinked but also into an eruptive state. As shown in Section VI, the evolution properties of magnetic helicity imply the spatial and temporal average of h_t must be zero for a non-eruptive steady-state solution for the magnetic field when $R_m \gg 1$ —no matter how spatially concentrated the current may become. Consequently, non-eruptive chaotic models tend to have spatially complicated distributions of Θ in which Θ has both signs and a near-zero spatial average as in the \vec{v}_t example used to construct Figure 2.

As discussed in Section V.B.1 of [28], the stability of force-free equilibria can be determined using the perturbed equilibrium equation $\vec{\nabla} \times \delta \vec{B} = (\mu_0 \delta j_{\parallel} / B) \vec{B}$, where $\delta \vec{B} = \vec{\nabla} \times (\delta A_{\parallel} \hat{z})$. The perturbed parallel current is determined by the constancy of $K \equiv \mu_0 j_{\parallel} / B$ along magnetic field lines, which in linear order in the perturbation implies $\vec{B} \cdot \vec{\nabla} \delta K + \delta \vec{B} \cdot \vec{\nabla} K = 0$. Stability is determined by whether it takes positive or negative energy to drive a perturbation that obeys the equations

$$\nabla_{\perp}^2 \delta A_{\parallel} = -\delta K B_0; \quad (40)$$

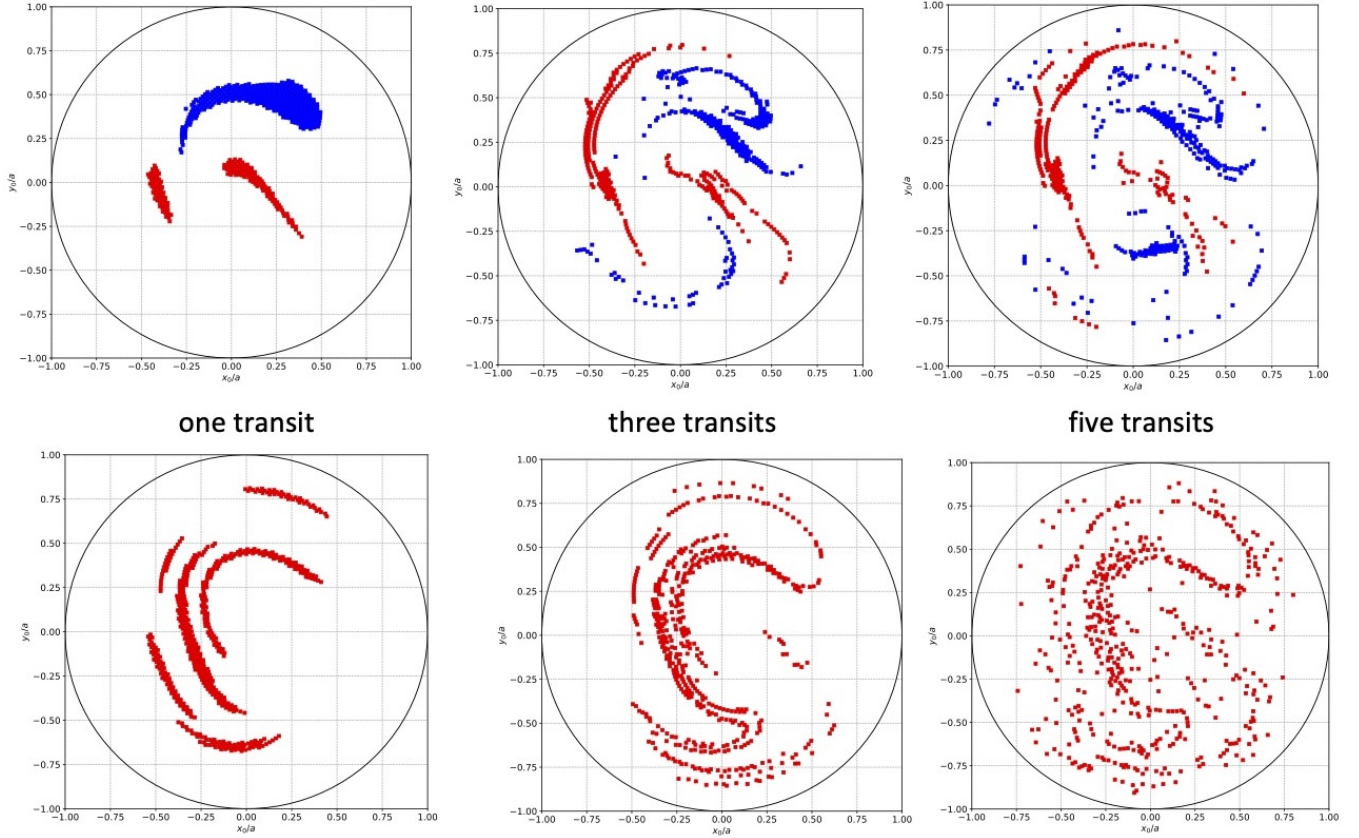
$$B_0 \left(\frac{\partial \delta K}{\partial \ell} \right)_{x_0 y_0} = \hat{z} \cdot \left(\vec{\nabla}_{\perp} A_{\parallel} \times \vec{\nabla}_{\perp} K \right). \quad (41)$$

The system is at marginal stability when δK is just strong enough to produce a solution δA_{\parallel} that fits within the perfectly conducting cylindrical walls. The implication is that when Equation (40) is multiplied by δA_{\parallel} , then at marginal stability

$$\int \left\{ \left(\vec{\nabla}_{\perp} \delta A_{\parallel} \right)^2 - \delta K \delta A_{\parallel} B_0 \right\} d^3 x = 0. \quad (42)$$

When δK has only a rapid spatial variation, as it does when K does, then δA_{\parallel} must also have a rapid variation to avoid a self-cancellation of the destabilizing term $\delta K \delta A_{\parallel}$ in Equation (42). Equation (41) for δK involves two spatial derivatives across \vec{B} and

Locations of large currents densities



Locations of rapid streamline separations

FIG. 5: Ten thousand starting points were uniformly spread over $r < a$. The top row is the locations of the five hundred points that had the largest current density $|K|$ after one, three, and five transits. Red implies K is negative and blue positive. The bottom row is the locations of the five hundred points that had the largest Frobenius norm, which measures the rapidity of streamline separation. The correlation between a large K and a large Frobenius norm is weak. The regions with a high current density K tend to become long and thin, but small regions that have a correlated current density do not entirely disappear. Figure 2c also illustrates this.

one might think they could be large and balance the stabilizing effect of the two spatial derivatives in $(\vec{\nabla}_{\perp} \delta A_{\parallel})^2$, but that is not the case. The two spatial derivatives across \vec{B} in the equation for δK are orthogonal and the spatial derivatives of K in the two directions across the magnetic field lines tend to be of exponentially different magnitudes, so the large term in $\vec{\nabla}_{\perp} K$ forces a large spatial derivative in δA_{\parallel} , which quadratically enhances $(\vec{\nabla}_{\perp} \delta A_{\parallel})^2$ but only linearly enhances δK .

V. MAGNETIC FLUX

The change in the magnetic flux associated with a particular magnetic field line $\psi(x_0, y_0, t)$ is the integral from one perfectly conducting surface to the other, $\partial\psi/\partial t = -\int \vec{E} \cdot d\vec{\ell}$. When the cylindrical conductor is stationary and the plasma is resistive, the flux decays as $\partial\psi/\partial t = -\int \eta \vec{j} \cdot d\vec{\ell}$.

As was shown in the derivation of Equation (15) for $\partial\vec{A}/\partial t$, the effective inductive electric field along the magnetic field is $-\vec{B} \cdot (\partial\vec{A}/\partial t) = \vec{B} \cdot (B_0 \vec{\nabla} h)$, which gives a change in the flux, $\partial\psi/\partial t = -\int \vec{E} \cdot d\vec{\ell}$, or

$$\frac{\partial\psi}{\partial t} = -B_0 h_t(x_0, y_0, t) \quad (43)$$

since the at the top of the cylinder $h = h_t$.

The appearance of $B_0 h_t$ in the electric-field integral can be understood using the expression $\vec{E} = -\vec{v}_t \times \vec{B}_0$ for the electric field in the flowing conductor when observed from a stationary frame of reference. The velocity is $\vec{v}_t = \hat{z} \times \vec{\nabla} h_t$ and $\vec{B}_0 = B_0 \hat{z}$, so $\vec{E} = -B_0 \vec{\nabla}_\perp h_t$. The electromotive force from the intersection point of the field line to a stationary point, where $h_t = 0$, is $B_0 h_t$.

The rate at which plasma resistivity destroys magnetic flux is $\mathcal{E}_\eta = \int \eta j_{||} dl$. Since $K = \mu_0 j_{||} / B$ is constant along a magnetic field line, $\mathcal{E}_\eta = B_0 (\eta / \mu_0) K(x_0, y_0, t) L$. Equation (35) implies $\partial \mathcal{E}_\eta / \partial t = -B_0 (\eta / \mu_0) \Omega_t(x_0, y_0, t)$. Since $\Omega_t = \nabla^2 h_t$, the ratio of flux creation to flux destruction is

$$\left| \frac{2 \partial h_t / \partial t}{(\eta / \mu_0) \nabla^2 h_t} \right| \approx R_m \sim 10^{12} \quad (44)$$

in the solar corona.

VI. MAGNETIC HELICITY

As will be shown, an argument based on magnetic helicity implies that a long-term relevant solution to the problem outlined in Figure 1 requires the long-term spatial and temporal average of h_t to be zero. When the average of h_t is zero over a chaotic region, the interchange of penetration points implies the poloidal magnetic flux associated with a field line x_0, y_0 fluctuates but has no systematic increase.

Chaotic streamlines can cause two field lines that penetrate the bottom of the cylinder at two distinct points x_0, y_0 and x'_0, y'_0 to interchange their penetration points through the top plane due to exponentially small non-ideal effects.

Equation (54) for the evolution of the magnetic helicity limits the degree to which a magnetic field driven as in Figure 1 can be simplified by magnetic field lines exchanging connections even if the current density were to obtain arbitrarily high local values by being concentrated in thin sheets. As has been shown, the maximum current density increases only linearly in time, Equation (37), and does not reach the enhancement by a factor of order $1/R_m$, which would be required for the loop voltage to balance the poloidal flux creation, before reconnection has already occurred. But, even if it did the rate of helicity dissipation would not be significantly enhanced, Equation (54). Magnetic turbulence can reduce the magnetic energy, but not the helicity [29, 30] as $R_m \rightarrow \infty$.

Equation (52) for the rate of helicity increase implies that unless the stream function integrated over each chaotic region, $\int h_t da_t$, has a zero time average, the magnetic helicity can increase without limit. In

the model of this paper, the perfectly conducting cylindrical boundary conditions will keep the system confined no matter how strong or contorted the magnetic field may become. But, in a natural system, such as the solar corona, a drive h_t that does not have a zero long-term average will presumably cause the eruption of a magnetic flux tube.

The derivation of the helicity evolution equation starts with the definition of the magnetic helicity enclosed by the cylinder,

$$\mathcal{K} \equiv \int \vec{B} \cdot \vec{A} d^3 x. \quad (45)$$

Equations (13) and (14) together with $\vec{\nabla} \cdot \vec{x}_\perp = 2$ imply $\vec{B} \cdot \vec{A} = B_0^2 (-2H + \vec{\nabla}_\perp \cdot (H \vec{x}_\perp))$. The helicity is then

$$\mathcal{K} = -2B_0^2 \int H d^3 x. \quad (46)$$

The time derivative of the helicity is calculated using

$$\begin{aligned} \frac{\partial \vec{B} \cdot \vec{A}}{\partial t} &= \vec{B} \cdot \frac{\partial \vec{A}}{\partial t} + \vec{A} \cdot \vec{\nabla} \times \frac{\partial \vec{A}}{\partial t} \\ &= 2\vec{B} \cdot \frac{\partial \vec{A}}{\partial t} - \vec{\nabla} \cdot \left(\vec{A} \times \frac{\partial \vec{A}}{\partial t} \right) \end{aligned} \quad \text{and (47)}$$

$$\vec{A} \times \frac{\partial \vec{A}}{\partial t} = -B_0^2 \frac{\vec{x}_\perp}{2} \frac{\partial H}{\partial t}, \quad \text{so} \quad (48)$$

$$\frac{\partial \vec{B} \cdot \vec{A}}{\partial t} = 2\vec{B} \cdot \frac{\partial \vec{A}}{\partial t} + \vec{\nabla} \cdot \left(B_0^2 \frac{\vec{x}_\perp}{2} \frac{\partial H}{\partial t} \right) \quad (49)$$

The side of the cylinder is a rigid perfect conductor, so $\partial H / \partial t = 0$ within its sides. Consequently,

$$\frac{d\mathcal{K}}{dt} = 2 \int \vec{B} \cdot \frac{\partial \vec{A}}{\partial t} d^3 x \quad (50)$$

$$= -2B_0 \int \vec{\nabla} \cdot (h \vec{B}) d^3 x \quad (51)$$

$$= -2B_0^2 \int h_t da_t, \quad (52)$$

using Equation (15) with $da_t = r dr d\theta$ the area integral over the top of the cylinder. Since the magnetic field lines are tied to the flow of the perfectly conducting top, $h = h_t$ within the top surface.

The effect of resistivity on the helicity is obtained by letting $\partial \vec{A} / \partial t = \vec{u}_\perp \times \vec{B} - B_0 \vec{\nabla} h - \eta \vec{j}$, then Equation (52) implies

$$\frac{d\mathcal{K}}{dt} = -B_0^2 \int \left(h_t + \frac{\int \eta j_{||} dl}{B_0} \right) da_t \quad (53)$$

$$= -B_0^2 \int \left(h_t + \int \frac{\eta}{\mu_0} K dl \right) da_t. \quad (54)$$

The effect of resistivity on the helicity evolution is given by the volume-averaged K , and is therefore unaffected by K being concentrated. When the evolution is slow compared to the Alfvén transit time, K is independent of ℓ , and the ratio of helicity input to its resistive destruction is

$$\left| \frac{h_t}{\int \frac{\eta}{\mu_0} K d\ell} \right| \sim \frac{av_t}{\frac{\eta}{\mu_0} L \frac{v_t}{a^2 L}} \sim \left(\frac{\mu_0 a^2}{\eta} \right) \left(\frac{v_t}{a} \right) \frac{a/v_t}{t} \quad (55)$$

$$\sim R_m \frac{a/v_t}{t}, \quad (56)$$

while $R_m \sim 10^{12}$ in the corona. To extreme accuracy, resistivity has no effect on the rate of helicity increase in the corona.

VII. POWER INPUT

The condition $\vec{\nabla} \cdot \vec{j} = 0$ implies that the Lorentz force $\vec{f}_L \equiv \vec{j} \times \vec{B}$ obeys Equation (28). Using

$$\vec{B} \cdot \vec{\nabla} K = B_0 \frac{\partial K}{\partial \ell} = -K\delta(\ell - L) \quad (57)$$

$$= B_0 \frac{\mu_0}{B_0^2} \hat{z} \cdot \vec{\nabla} \times \vec{f}_L, \quad (58)$$

$$\hat{z} \cdot \vec{\nabla} \times \vec{f}_L = -\frac{B_0^2}{\mu_0} K\delta(\ell - L). \quad (59)$$

The power required to maintain the flow in the top of the cylinder is

$$\begin{aligned} \mathcal{P} &= - \int \vec{v}_t \cdot \vec{f}_L d^3x \quad (60) \\ &= - \int \hat{z} \cdot (\vec{\nabla} h_t \times \vec{f}_L) d^3x \\ &= - \int \hat{z} \cdot \left(\vec{\nabla} \times (h_t \vec{f}_L) - h_t \vec{\nabla} \times \vec{f}_L \right) d^3x \\ &= - \int \hat{z} \cdot \left(-\vec{\nabla} (h_t \hat{z} \times \vec{f}_L) \right. \\ &\quad \left. + \frac{B_0^2}{\mu_0} h_t K\delta(\ell - L) \right) d^3x \\ &= - \frac{B_0^2}{\mu_0} \int h_t(x_0, y_0, t) K(x_0, y_0, t) dx_0 dy_0. \quad (61) \end{aligned}$$

The integrand becomes extremely spatially complicated as time evolves but is not very large.

VIII. DISCUSSION

The prevalence of magnetic reconnection in situations in which effects that cause a departure from

an ideal evolution are arbitrarily small suggests the cause of reconnection must be within the ideal evolution equation itself. Indeed it is [4].

In an ideal evolution, the magnetic field lines move with the velocity \vec{u}_\perp of Equation (1). As Schindler, Hesse, and Birn [7] stated in 1988, resistivity η can only compete with the ideal evolution in a region Δ_d that is sufficiently narrow across the magnetic field that the local magnetic Reynolds number, $R_\ell = (\mu_0 u_\perp / \eta) \Delta_d \sim 1$. The actual scale of the reconnecting region across the magnetic field, a , gives the usual magnetic Reynolds number $R_m = (\mu_0 u_\perp / \eta) a$, which is many orders of magnitude larger than unity—in both natural and laboratory plasmas. In the solar corona $R_m \sim 10^{12}$. There are two possibilities for addressing the $a/\Delta_d \sim R_m$ problem identified by Schindler et al.

The first possibility, which is the dominant reconnection paradigm and the only one considered by Schindler et al, is that the ideal magnetic evolution creates and maintains layers of intense current density $j \sim B_{rec}/\mu_0 \Delta_d$, where B_{rec} is the reconnecting magnetic field. One problem with this possibility is that in an ideal evolution the current density tends to increase only linearly in time. A linear increase in the current density by a factor R_m takes far too long to explain many natural phenomena. The growth in current density is found to be linear in time, not only in this paper, Equation (37), but also in ideal flows that are known to create a singular current density as time goes to infinity—flows that have a resonant interaction with a rational magnetic surface in a torus [12, 24]. Although more complicated than a linear increase, a slow increase in current density along the magnetic field lines is also found for lines that pass near a magnetic null [13].

What has been presented in this paper is an example of the second possible explanation for fast magnetic reconnection, but one that has aroused little interest. This explanation is based on the characteristic increase in the ratio of the maximum to the minimum separation, $\Delta_{max}/\Delta_{min}$, between two magnetic lines that is produced by an ideal flow \vec{u}_\perp . Magnetic field lines are defined at a fixed time, as is $\Delta_{max}/\Delta_{min}$, but when the two lines are adjacent at some location along their trajectories, $\Delta_{min} \rightarrow 0$, the $\Delta_{max}/\Delta_{min}$ ratio characteristically increases exponentially when the field-line trajectories are calculated at different points in time. Characteristically, the rate of exponentiation is comparable to the evolution time $\tau_{ev} \equiv a/u_\perp$. Reconnection must have occurred by the time at which $\Delta_{max}/\Delta_{min} \sim R_m$ with $\Delta_{min} = \Delta_d$, the spatial scale over which field line distinguishability is lost, and $\Delta_{max} \sim a$, the system scale.

All that is required to produce reconnection by the

Parker and Krook definition [2], the “*severing and reconnection of lines of force*,” is that magnetic field lines become indistinguishable on some spatial scale Δ_d and that the exponentiation of field-line separation magnify the indistinguishability scale to the scale over which reconnection occurs. Indeed, one can model magnetic reconnection using an ideal code [31] because finite numerical resolution will provide an effective distinguishability scale Δ_d . In many examples of reconnection, the distinguishability scale Δ_d is far smaller than can be directly assessed numerically. It is important to carry out reconnection studies minimizing effects that break the ideal magnetic evolution.

Unlike a localized current density, $\Delta_{max}/\Delta_{min}$ becomes large over extended regions. Nonetheless, the exponentiation, which is quantified by the Frobenius norm, Section II C, differs from one pair of magnetic field lines to another—even over small regions, Figure 2b. Magnetic field lines that have the largest exponentiations reconnect first, which can break force-balance and cause Alfvénic relaxations when the reconnected region becomes sufficiently large, which is the scale Δ_r at which reconnection becomes important to the system dynamics. The scale Δ_r is important but not determined in this paper. That would require more complete simulations related to those of Reid et al [17], and Δ_r is far less well defined than the distinguishability scale Δ_d . Nonetheless, Δ_r is an important concept because the typical size of reconnected regions scale as Δ_d times a factor that depends exponentially on time until the scale of reconnection reaches Δ_r , then reconnection spreads at an Alfvénic rate, which presumably accounts for Parker’s observation [32] that the speed of reconnection is $\approx 0.1V_A$. Even though an Alfvénic relaxation is consistent with an ideal evolution, it generally causes an increase in $\Delta_{max}/\Delta_{min}$ on the Alfvénic time scale for pairs of magnetic field lines in additional regions of space.

Plasma turbulence can be considered to be third possibility for fast reconnection, but turbulence-enhanced reconnection is in effect given by one of the other two possibilities. Plasma turbulence can mean either micro-turbulence or macro-turbulence: (1) Micro-turbulence affects the particle distributions of the Fokker-Planck equation and can cause an enhanced turbulent resistivity η_{turb} for the flow of current along \vec{B} , which can be much larger than the standard Spitzer value for the parallel resistivity, η . This effect fits into the paradigm of Schindler, Hesse, and Birn [7]; just $\eta_{turb}j_{\parallel}$ must compete with the evolution rather than ηj_{\parallel} . (2) Macro-turbulence means the mass flow velocity of the plasma \vec{v} develops small spatial scales with no direct effect on the particle distribution function. Macro-turbulence is

analogous to the turbulent flow of water through a pipe.

In 1953 Dungey [33] stated that a change in the linkages of magnetic field lines due to resistivity “*is usually very slow in astrophysical systems, but may be increased by turbulent motion in the gas*.” The literature on macro-turbulence enhanced reconnection is extensive; a few papers are [34–39], and [40] is a review.

Macro-turbulent enhanced reconnection has the same relation to enhanced reconnection due to the exponentiation of field line separations as the pre-Aref theories of fluid mixing to that of Aref [10]. When macro-turbulence is three dimensional, it does cause the magnetic field to become chaotic. Nevertheless when the characteristic spatial scale of the turbulent eddies ℓ_{turb} is small compared to the scale a over which strong advection takes place, the advection from the eddies behaves as a diffusive process [9]. The diffusive advection of the turbulent eddies is much slower than the advective transport due to flows that have a scale comparable to a unless the maximum flow speed is far larger than the flow speed averaged over the scale ℓ_{turb} . A turbulent ideal flow \vec{u}_{\perp} does not directly produce magnetic reconnection any more than a laminar flow does; both cause an exponentially enhanced sensitivity to non-ideal effects.

The simple model of developed here illustrates how the laminar flow of an ideal magnetic evolution can force magnetic reconnection on a time scale that is the ideal evolution time, $\tau_{ev} \equiv a/u_{\perp}$ times the logarithm of the ratio of the intrinsic magnitude of the ideal to the connection breaking terms.

A spatially bounded flow of a footpoint of a magnetic field line that has a smooth and slow variation in space and time can be chaotic and impart what many may find to be surprising properties to the magnetic field lines in an ideal evolution. The other footpoint of the line is assumed to fixed in space.

Two magnetic field lines that are separated by the distance Δ_{min} at the stationary foot point must have a maximum separation Δ_{max} at least as great as the separation of the lines at the moving footpoint. The separation of neighboring streamlines determines the minimum $\Delta_{max}/\Delta_{min}$ ratio that the two magnetic field lines must have obtained. Figure 4c shows that no matter how small Δ_{min} may be that Δ_{max} will reach a value comparable to a , the distance scale of the system perpendicular to the magnetic field, within a time that depends only logarithmically on Δ_{min} . Identifying Δ_{min} with the spatial scale Δ_d on which magnetic field lines become indistinguishable, the time required for large-scale reconnection to occur is the evolution time defined by the footpoint flow speed times a logarithmic factor depend-

ing on a/Δ_d . This argument assumes the reconnection scale Δ_r is comparable to a , although it could be smaller, which would imply large scale reconnection would occur even sooner.

Many more properties of an ideally evolving magnetic field can be determined from the footpoint motion when its evolution time is long compared to the time for an Alfvén wave to propagate from one footpoint interception to the other and the magnetic field remains kink stable. The example of the footpoint flow that was studied was chosen to be consistent with the maintenance of kink stability. Two properties that can be determined are the distribution of the current density $K \equiv \mu_0 j_{\parallel}/B$, which is constant along the magnetic field lines under these conditions, and the power that is required to drive the footpoint flow. The figures show the quantity KL rather than K because KL is the quantity that is determined by the theory; not K and L separately. $KL/2$ is the dimensionless twist angle that a magnetic field line makes in going between the two footpoints of each field line, which are separated by the distance L .

Despite the smoothness and simplicity of the footpoint flow that was studied, the current density distribution K varies wildly among field lines that have their stationary footpoints in a tiny region, Figure 2c. The currents in the corona must be extremely complicated with a short correlation distance across the magnetic field lines. Observations of spatial complexity in the current density are clearly not a proof of turbulence. Nearby magnetic field lines can have currents flowing in opposite directions. In addition the magnitude of K increases only linearly in time, Figure 2c, and forms ribbons along the magnetic field that tend to widen exponentially and thin as one over the exponential, Figure 5. As discussed in Appendix E of [18], the currents produced by the more localized photospheric motions could produce runaway electrons and explain the hot corona.

To be consistent with Ampere’s law, K must have a typical magnitude that is proportional to the logarithm of the exponentiation factor [26]. A heuristic argument is given in Section IIID. The exponentiation factor is the Frobenius norm of a Jacobian matrix, Section IIC. This approximate proportionality is illustrated in Figure 4c and requires the current density be enhanced by factor of $\ln(R_m)$ above its characteristic value before reconnection due to exponentially enhanced resistive diffusion can compete with evolution. An enhancement of the current density by $\ln(R_m) \sim \ln(10^{12}) \approx 28$ is modest compared to an enhancement by $R_m \sim 10^{12}$. Despite this relationship between K and the Frobenius norm, the regions in which they are particularly large are not closely correlated. Reid et al [19] also found a weak

correlation between the current density j_{\parallel} and ratio at the two footpoint locations of the distance between neighboring field lines, which is the definition of the quasi-squashing factor [41, 42].

The power required to drive the footpoint motion, Section VII, is a spatial average of the footpoint motion times the current distribution K , so it increases approximately linearly in time and never becomes extremely large.

Section VI demonstrated that unless the stream function $h_t(x, y, t)$, which defines the footpoint flow, has a zero spatial and temporal average over a footpoint region, the magnetic helicity increases without limit in the volume occupied by the magnetic field lines that strike that region. When $R_m \gg 1$, magnetic helicity cannot be destroyed faster than it is created in such regions—even by macro-turbulence—and the result must be the ejection of a magnetic flux tube, called a plasmoid, from the region.

The example of a footpoint flow that was discussed here had a very simple and smooth spatial and temporal dependence; realistic footpoint motions of coronal loops are far more complicated, which makes them more prone to chaos. However, the parts of the footpoint motion that cause the most rapid development of states in which large-scale reconnection is inevitable have a spatial scale comparable to the region a over which reconnection will take place.

The calculations made in this paper demonstrate that a magnetic field reaches a state in which reconnection is inevitable on a time scale that is only logarithmically longer than the ideal evolution time scale, even when drive for the evolution is simple.

Nonetheless, more complete simulations related to those of Reid et al [17], are required for a more complete understanding of how the reconnection proceeds. It is particularly important to use such simulations to understand how the magnetic reconnection region is determined, not because it is bounded by a rigid conductor but by unstressed magnetic field lines. This can be done by choosing a non-zero λ^2 in Equation (5). As λ^2 is made larger within the model of this paper, simulations become more expensive but more representative of the corona. Such simulations are numerically simpler when the circular cylinder of Figure 1 is replaced by a cylinder of square cross section that encloses the volume with $|x| < a$, $|y| < a$, and $0 < z < L$. As mentioned at the end of Section IIB, the only significant modification required is a change in the factors of $1 - r^2/a^2$ in Equation (5) to $(1 - x^2/a^2)(1 - y^2/a^2)$.

Acknowledgements

This work was supported by the U.S. Department of Energy, Office of Science, Office of Fusion Energy Sciences under Award Numbers DE-FG02-95ER54333, DE-FG02-03ER54696, DE-SC0018424, and DE-SC0019479.

Data availability statement

The data that support the findings of this study are available from the corresponding author upon reasonable request.

-
- [1] P. Cargill (2015), *Magnetic Reconnection in the Solar Corona: Historical Perspective and Modern Thinking*. In: Cowley FRS S., Southwood D., Mitton S. (eds) *Magnetospheric Plasma Physics: The Impact of Jim Dungey's Research*, Astrophysics and Space Science Proceedings, vol 41, Springer, Cham.
- [2] E. N. Parker and M. Krook, *Diffusion and severing of magnetic lines of force*, *Ap. J.* **124**, 214 (1956).
- [3] W. A. Newcomb, *Motion of magnetic lines of force*, *Ann. Phys.* **3**, 347 (1958).
- [4] A. H. Boozer, *Fast magnetic reconnection and the ideal evolution of a magnetic field*, *Phys. Plasmas* **26**, 042104 (2019).
- [5] L. Spitzer, *Physics of Fully Ionized Gases*, second edition (John Wiley and Sons, New York, 1962). See Equation (2-12).
- [6] A. H. Boozer, *Magnetic Reconnection with null and X-points*, *Phys. Plasmas* **26**, 122902 (2019).
- [7] K. Schindler, M. Hesse, and J. Birn, *General magnetic reconnection, parallel electric-fields, and helicity*, *Journal of Geophysical Research—Space Physics* **93**, 5547 (1988).
- [8] D. A. Uzdensky, N. F. Loureiro, and A. A. Schekochihin, *Fast Magnetic Reconnection in the Plasmoid-Dominated Regime*, *Phys. Rev. Lett.* **105**, 235002 (2010).
- [9] A. H. Boozer, *Magnetic reconnection and thermal equilibration*, *Phys. Plasmas* **28**, 032102 (2021).
- [10] H. Aref, *Stirring by chaotic advection*, *Journal of Fluid Mechanics* [143], 1 (1984).
- [11] H. Aref, J. R. Blake, Marko Budisić, S. S. S. Cardoso, J. H. E. Cartwright, H. J. H. Clercx, K. El Omari, U. Feudel, R. Golestanian, E. Guillard, G. J. F. van Heijst, T. S. Krasnopolskaya, Y. Le Guer, R. S. MacKay, V. V. Meleshko, G. Metcalfe, I. Mezić, A. P. S. de Moura, O. Piro, M. F. M. Speetjens, R. Sturman, J.-L. Thiffeault, and I. Tuval, *Frontiers of chaotic advection*, *Rev. Mod. Phys.* **89**, 025007 (2017).
- [12] T. S. Hahm and R. M. Kulsrud, *Forced magnetic reconnection*, *Phys. Fluids* **28**, 2412 (1985).
- [13] T. Elder and A. H. Boozer, *Magnetic nulls in interacting dipolar fields*, <https://arxiv.org/pdf/2005.08242.pdf>, accepted for publication by the Journal of Plasma Physics.
- [14] E. N. Parker EN (1972) *Topological dissipation and the small-scale fields in turbulent gases*, *Astrophys. J.* **174**, 499 (1972).
- [15] David I. Pontin and Gunnar Hornig, *The Parker problem: existence of smooth force-free fields and coronal heating*, *Living Reviews in Solar Physics* **17**, 5 (2020).
- [16] A. H. Boozer, *Why fast magnetic reconnection is so prevalent*, *Journal of Plasma Physics* **84**, 715840102 (2018).
- [17] J. Reid, A. W. Hood, C. E. Parnell, P. K. Browning, and P. J. Cargill, *Coronal energy release by MHD avalanches: continuous driving*, *Astronomy and Astrophysics* **615**, A84 (2018).
- [18] A. H. Boozer, *Fast magnetic reconnection and particle acceleration*, *Phys. Plasmas* **26**, 082112 (2019).
- [19] J. Reid, C. E. Parnell, A. W. Hood, and P. K. Browning, *Determining whether the squashing factor, Q , would be a good indicator of reconnection in a resistive MHD experiment devoid of null points*, *Astronomy and Astrophysics* **633**, A92 (2020).
- [20] D. Borgogno, D. Grasso, F. Pegoraro, and T. J. Schep, *Barriers in the transition to global chaos in collisionless magnetic reconnection. I. Ridges of the finite time Lyapunov exponent field*, *Phys. Plasmas* **18**, 102307 (2011).
- [21] Yi-Min Huang, A. Bhattacharjee, and A. H. Boozer, *Rapid change of field line connectivity and reconnection in stochastic magnetic fields*, *Ap. J.* **793**, 106 (2014).
- [22] B. B. Kadomtsev and O. P. Pogutse, *Nonlinear helical perturbations of a plasma in the tokamak*, *Sov. Phys.-JETP*, **38**, 283 (1974).
- [23] H. R. Strauss, *Nonlinear, 3-dimensional magneto-hydrodynamics of noncircular tokamaks*, *Phys. Fluids* **19**, 134 (1976).
- [24] A. H. Boozer and N. Pomphrey, *Current density and plasma displacement near perturbed rational surfaces*, *Phys. Plasmas* **17**, 110707 (2010).
- [25] A. H. Boozer, *Flattening of the tokamak current profile by a fast magnetic reconnection with implications for the solar corona*, *Phys. Plasmas* **27**, 102305 (2020).
- [26] A. H. Boozer, *Separation of magnetic field lines*, *Phys. Plasmas* **19**, 112901 (2012).
- [27] A. W. Hood and E. R. Priest, *Kink instability of solar coronal loops as the cause of solar flares*, *Solar Physics* **64**, 303 (1979).
- [28] A. H. Boozer, *Physics of magnetically confined plasmas*, *Rev. Mod. Phys.* **76**, 1071 (2004).
- [29] J. B. Taylor, *Relaxation of Toroidal Plasma and Generation of Reverse Magnetic Fields*, *Phys. Rev. Lett.* **33**, 1139 (1974).
- [30] M. A. Berger, *Rigorous new limits on magnetic helicity dissipation in the solar corona*, *Geophysical*

- and Astrophysical Fluid Dynamics, **30**, 79 (1984).
- [31] E. Pariat, S. K. Antiochos, and C. R. DeVore, *A model for solar polar jets*, Ap. J. **691**, 61 (2009).
- [32] E. N. Parker, *The reconnection rate of magnetic fields*, Ap. J. **180**, 247 (1973).
- [33] J. W. Dungey, *The motion of magnetic fields*, Monthly Notices of the Royal Astronomical Society **113**, 679 (1953).
- [34] A. Lazarian and E. T. Vishniac, *Reconnection in a weakly stochastic field*, Ap. J. **517**, 700 (1999).
- [35] G. L. Eyink, A. Lazarian, E. T. Vishniac, *Fast magnetic reconnection and spontaneous stochasticity*, Ap. J. **743**, 51 (2011).
- [36] G. L. Eyink, *Turbulent general magnetic reconnection*, Ap. J **807** 137 (2015).
- [37] W. H. Matthaeus, M. Wan, S. Servidio, A. Greco, K. T. Osman, S. Oughton, and P. Dmitruk, *Intermittency, nonlinear dynamics and dissipation in the solar wind and astrophysical plasmas*, Phil. Trans. R. Soc. A **373** 20140154 (2015).
- [38] G. Kowal, Di A. Falceta-Gonçalves, A. Lazarian, and E. T. Vishniac, *Kelvin-Helmholtz versus Tearing Instability: What Drives Turbulence in Stochastic Reconnection?*, Ap. J. **892**, 50 (2020).
- [39] S. Adhikari, M. A. Shay, T. N. Parashar, P. S. Pyakurel, W. H. Matthaeus, D. Godzieba, J. E. Stawarz, J. P. Eastwood, and J. T. Dahlin, *Reconnection from a turbulence perspective*, Phys. Plasmas **27**, 042305 (2020).
- [40] A. Lazarian, G. L. Eyink, A. Jafari, G. Kowal, H. Li, S-Y Xu, and E. T. Vishniac, *3D turbulent reconnection: Theory, tests, and astrophysical implications*, Phys. Plasmas **27**, 012305 (2020).
- [41] E. R. Priest and P. Démoulin, *Three-dimensional magnetic reconnection without null points: 1. Basic theory of magnetic flipping*, J. Geophys. Res., **100**, 23443 (1995).
- [42] V. S. Titov, G. Hornig, and P. Démoulin, *Theory of magnetic connectivity in the solar corona*, J. Geophys. Res., **107**, 1164 (2002).